Defence Science Journal, Vol. 59, No. 4, July 2009, pp. 413-424

Nano Pattern Formation and Surface Modifications by Ion Irradiation

Dipak Paramanik, Subrata Majumder, S.R. Sahoo, and Shikha Varma*

Institute of Physics, Bhubaneswar-751 005
**E-mail: shikha@iopb.res.in*

ABSTRACT

Ion Irradiation is a technologically important technique to modify the surfaces. We have investigated the patterning of InP(111) surfaces by low energy (3 keV) as well as high energy (1.5 Mev) ion beams. After low energy ion irradiation, surfaces exhibit well defined nano dots which ripen at initial stages but exhibit fragmentations at high fluences. The surface rms, at both the energies, displays a similar behaviour of initially increasing with increasing fluences but decreasing for higher fluences. The studies show some common features at these low and high energies, like the smoothening of surface beyond the a/c transition.

Keywords: InP, AFM, ion irradiation, nanotechnology, semiconductor nanostructures, fabrication

1. INTRODUCTION

Unique properties of InP have attracted enormous research interest. It is being widely applied in high speed electronic and opto-electronic devices due to its attractive electronic properties[1,2,3] as well as its excellent lattice match with low band gap alloys like GaInA*s*, GaInAsP, AlGaInAs, etc. GaInAsP/InP-based photo-diodes operate in low loss window of silica bers with high quantum e.ciency and fast response time. Due to its excellent physical properties like high thermal conductivity, high peak velocities for electrons and holes, InP is considered an important semiconductor material and it is being prominently utilized in the devices for high electron mobility transistors, high e.ciency and high speed quantum well lasers, photodetectors, photonic integrated circuits, etc. InP is also preferred, over GaAs based devices, for Millimeter-wave sources and ampli.ers due to its low noise and higher e.ciency operations in high frequency regime. Junction .eld e.ect transistors fabricated on InP display high performance.

With the fast growing interest in nanotechnology, fabrication of regular arrays of semiconductor nanostructures with controlled size and height is highly desirable. These nanoscale pattern hold promise in applications as varied as optical devices, templates for liquid crystal orientation, and strain-free patterned substrates for heteroepitaxial growth of quantum dots or wires[4]. Fabrication of nano-dots through self-organization induced by low (keV) energy 1 ion irradiation processes has attracted special interest due to the possibility of production of regular arrays of dots on large areas in a single technological step. The pattern formation is related to the surface instability between curvature dependant ion sputtering that roughens the surface and smoothening by different relaxation mechanisms[5-8]. Recently it was observed that self organized patterns can evolve from low energy ion sputtering of III-V semiconductor surfaces. This patterning is mostly performed either under normal incidence conditions[8-10] or in off-normal geometry coupled with rotation[11,12]. Generally for off-normal ion incidence, without sample rotation, a periodic height modulation in the form of ripple or wave like structure, with sub-micron length scale, develops during ion bombardment as observed for single crystalline III-V semiconductors[13,14].

Based on Sigmund's continuum theory of ion-beam sputtering[5] recently, Cuerno and Barabasi (CB)[15] or more generally, Makeev, Cuerno, and Barabasi (MCB)[16] have developed a model to describe the ion-induced pattern formation on amorphous or semiconductor materials that are easily amorphized by ion bombardment. The early stage morphology predicted by the CB model[15] is similar to the linear instability theory developed by Bradley and Harper (BH)[6]. However, the late stage dynamics of the ion-induced morphology is dominated by the nonlinear terms of the Kuramoto-Sivashinsky (KS) equation[17] involved in the CB model[15] as described by Park[18], *et al*. and Rost and Krug[19]. Depending on the sign of the product of the coefficients of the two non- linear terms, the late stage morphology may show[15,18,19] kinetic roughening described by the universality class of the Kardar-Parisi-Zhang (KPZ) equation[20] or yield the formation of rotated ripple structure(RRS)[18,20] or display dots and hole[8-10] on the ion eroded surface. Starting from the Bradley-Harper (BH) theory[6], description of the morphological evolution of the ion sputtered surface can be given by the isotropic KS equation[9,10,15,19]. The temporal development of the surface profile h(x,y,t) is given by the following undamped KS equation:

Received 12 January 2009

$$\frac{\partial h}{\partial h} = -V_0 + V\nabla^2 h - D_{eff}\nabla^4 + \frac{\lambda}{2}(\nabla h)^2 + \eta \quad (1)$$

where V_0 is the constant erosion velocity and V is the effective surface tension, caused by the erosion process, which usually has a negative value leading to a surface instability. D_{eff} is the surface diffusion coeffcient which is the sum of thermal diffusion and ion inducedeffective diffusion. The nonlinear term $\frac{\lambda}{2}(\nabla h)^2$ accounts for the slope-dependent erosionyield that brings forth the saturation of surface roughness with time. η is an uncorrelated white noise with zero mean, mimicking the randomness resulting from the stochastic nature of ion arrival to the surface.

MeV ion-beam implantation techniques are extensively utilized for device processing in semiconductor industry. Due to its low thermal stability, MeV ion implantation is a prominent way to introduce and dope the materials in InP. MeV implantation is also important for forming thick buried layers with modified properties as well as modifcation of vertically limited layers and quantum well structures. The increased density in VLSI circuits also makes the technological applications of the ion implantation, especially in MeV energy range, increasingly important. *Sb* is considered an important dopant because of its role in the development of field effect transistors and infrared detectors[21]. *Sb* has also found applications as isoelectronic dopant for trapping charge carriers in InP[22]. MeV implantation, however, can also produce severe modifications in the material depending on the nature and the energy of the impinging ion, and the implantation dose[23]. Extensive usage of ion implantation in device fabrication and the continued miniaturization of device structures has brought the issue of surface modifications, via ion implantations, to the forefront. However, the factors responsible for such modifcations and the surface morphology after ion implantation, have received little attention[24]. These issues are important from fundamental as well as technological point of view for ion implantation to be a viable candidate for the development in semiconductor technology. Since roughness of surface can crucially effect the performance and reliability of devices[25], it becomes necessary to characterize the surface roughness and understand the processes influencing it. The formation and the development of the surface structures, due to the ion implantation, are also gaining importance because of the realisation that these structures can be utilized for controlled fabrication of semiconductors similar to self-organized growths.

During implantation, a projectile while moving forward produces defects and loses energy due to scattering processes. The ion gets finally deposited at the range governed by its mass and implant energy[26]. At MeV energies, nuclear energy loss (S_n) processes are expected to be dominantly responsible for the material modiffications. Defects and strains can get produced, via S_n, causing the modifications in the surface and bulk properties[27,28].

In this paper we reporte our studies on the pattern formations on the InP(111) surfaces utilizing the ion irradiation. We notice that the keV irradiation leads to the formation of nanodots on the InP surfaces. The sputtering phenomenon, causing the systematic removal of surface atoms, dominates during the keV irradiation. Sputtering of the InP has been carried out by 3 keV *Ar* ions at room temperature. The nano-dots have been produced over a wide temporal range of sputtering time spanning from 5 min. to 80 min., with a low ion flux of 1×10^{13} ions $cm^{-2}s^{-1}$. Here we present a detailed investigation on the temporal evolution and the coarsening behaviour of InP nano dots in conjunction with the structural modifications occurring on the InP(111) surface. The average size and height of the nanostructures vary in the range of 10 to 100 nm and 5 to 40 nm, respectively, for diferent sputtering times. A high density of nano-dots, with narrow size and height distributions, is found for 10 min. of sputtering. These nano-dots exhibit a weak short range ordering. They coarsen and agglomerate with increasing sputtering time. The dots display their largest size after 40 min. of sputtering which denotes a critical sputtering time, as for larger durations a fragmentation of the dots with a decrease in their sizes is observed. During this nano dot formation, by ion beam irradiation, the surface undergoes several modifications. The associated rms roughness of InP surfaces also displays a critical time with the roughness increasing during the coarsening regime of the dots, where the dots grow in size, up to the critical time but decreasing beyond it. The surface also exhibits a tensile stress which reduces for sputtering durations larger that critical time. Raman Scattering results presented here show that the surface undergoes a crystalline to amorphous (c/a) phase transition for the critical sputtering time. The c/a transition promotes the fragmentation of the dots as well the stress relaxation for higher sputtering durations. The theoretical model based on linear BH or KS equations show that the characteristic surface roughness will saturate for long fluences. However, both the keV and MeV irradiated surfaces display that this surface roughness does not saturate but decreases for long fluences suggesting a smoothening of the surface at long durations. The salient features of our results, thus, suggest that BH or KS model does not describe the surface morphology, seen in the present experiments, completely and the inclusion of non-linear terms higher than those present in the KS theorys, may be essential for describing the observed surface evolution.

We also discuss the effect of MeV ion irradiation on the InP(111) surfaces. Here we have utilized the SPM technique to study the formation of nano-structures on the MeV irradiated InP(111) surfaces. These nanostructures evolve with time and are composed of damaged zones produced due to high energy irradiation. Here also, similar to the scenario after keV irradiation, the surface undergoes several modifcations. However, although the energy is higher and the nature of patterning is diferent from that seen at keV irradiation, a critical influence for c/a transition is again observed. The maximum rms surface roughness and the maximum surface stress are present at this critical fluence. Again as seen after keV irradiation, c/a transition occurs on the surface at the

critical Fluence leading to the relaxation of stress and a decrease in its roughness. These studies demonstrate that similar principles are guiding the formation of surface structures at two very different, keV and MeV, energies

2. EXPERIMENTAL

For keV irradiation studies, InP(111) wafers were sputtered by 3 keV Ar^+ ions in absence of any sample rotation. Sputtering was performed at an incidence angle of 15° wrt surface normal in a UHV chamber for 5 to 80 min. with a low ion flux of 1×10^{13} $cm^{-2}s^{-1}$ producing flunces in the range of 3×10^{15} to 4.8×10^{16} ions/cm^2. Nearly 200 images of 50 nm to 10 μm sizes of ion beam modi?ed surfaces were imaged in tapping mode by Nanoscope IIIA multimode mode Scanning Probe Microscope (SPM). The mean size, height and density of the nano dots were calculated from range of a statistics of around 500 dots for each sample using the Nanoscope software. Raman scattering measurements were performed at room temperature in the backscattering geometry, with a 488 nm argon ion laser at 500 mW, using a spectrometer with a liquid nitrogen cooled, charged coupled device (CCD) array as a detector.

For MeV irradiation studies also an InP(111) single crystal wafer was used. The samples were implanted at room temperature with a scanned beam of 1.5 MeV Sb^{2+} ions at various fluences ranging from 1×10^{11} to 5×10^{15} ions/cm^2. The average *Sb* flux was 0.02 μA/cm^2. This current was measured directly on the target after suppressing the secondary electrons by applying a negative bias of 200 V to a suppressor assembly around the target. The implantations were performed with the samples oriented 7° off-normal to the incident beam to avoid channeling effects. Monte Carlo simulations were performed for 1.5 MeV *Sb* implantation in InP using the SRIM'03 code and the mean projected range of *Sb*-ion distribution was found to be 400 nm[29]. Same SPM, as described above, was used to image the surface morphology of the InP(111) samples. Images ranging from 0.2 to 10 μm square were obtained. The root mean square (rms) surface roughness was calculated by the SPM software. Raman scattering measurements were performed using a SPEX 1877E Triplemate Spectrometer with a liquid nitrogen cooled CCD array. Raman experiments were carried out at room temperature using the 514 nm line of an Argon ion laser in the backscattering geometry. At this wavelength the penetration depth of the light is estimated to be about 100 nm.

3 RESULTS AND DISCUSSION

3.1 Nano-dots formation after keV Ion Irradiation

Figure 1 shows the two dimensional 500 nm×500 nm SPM images of InP surfaces sputtered for durations varying from 5 min. to 80 min. (fluences are shown in Fig. 1). An image from a virgin (un-sputtered) surface is also shown (Fig. 1(a)). After sputtering for 5 min some irregular structures, wavy patterns as well as some dots are seen on InP surfaces (Fig. 1(b)). However, after 10 min. sputtering the surface topography appears very different.

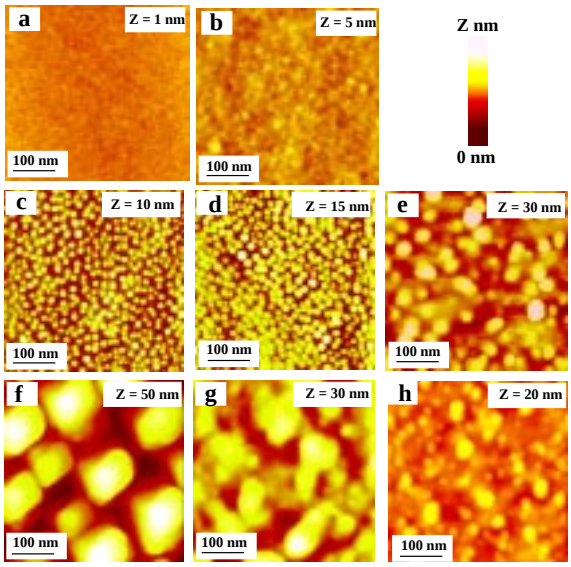

Figure 1. 500 × 500 nm^2 SPM images of InP surfaces for the virgin sample (a) as well as after sputtering it for 5 min (3×10^{15} ions/cm^2)(b), 10 min. (6×10^{15} ions/cm^2)(c), 20 min (12×10^{15} ions/cm^2)(d), 30 min (18×10^{15} ions/cm^2)(e), 40 min. (24×10^{15} ions/cm^2)(f), 60 min (36×10^{15} ions/cm^2) (g), and 80 min(48×10^{15} ions/cm^2) (h).

The surfaces display the presence of several nano dots (Fig. 1(c)). The size and the height distributions are shown in Figs. 2 and 3. The density of dots is found to be 2×10^{11} cm^2. The dots display a narrow size distribution with a mean dot diameter of 24 ± 4 nm and a mean height of 4 ± 0.4 nm (Fig. 3). Very small nano dots of sizes smaller than 13 nm and heights lower than 3.5 nm are also seen (Fig. 2). The autocorrelation image of the pattern in Fig. 1(c), for 10 min sputtering, is shown in Fig. 5(a). This image shows a weak short range ordering among the dots with the mean dot separation being 30 ± 4 nm. Although the density of the dots remains the same after a sputtering for 20 min (Fig. 1(d)), the dots appear to have slightly ripened and grown with the average diameter and the height

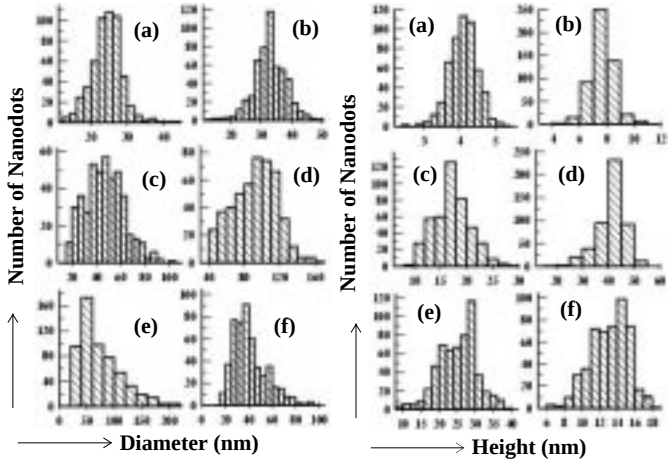

Figure 2. Size (a) and height (b) distributions of the nanostructures formed after sputtering.

being 32 nm and 8 nm, respectively (Fig. 3). The ripening of dots continues after the sputtering for 30 min also. At this stage, however, a drastic agglomeration of dots is also observed in Figure 1(d). As a result, a large increase in the size and height of dots is observed with their average diameter and height becoming 50 nm and 18 nm, respectively (Fig. 2). Nano dots smaller than 15 nm, seen after early stage of sputtering of 5 and 10 min are not observed at this stage. Moreover, several dots of sizes as large as 90 nm and heights as large as 27 nm can be seen. Both the height and size distribution have become broader due to the ripening and agglomeration of dots. As a consequence

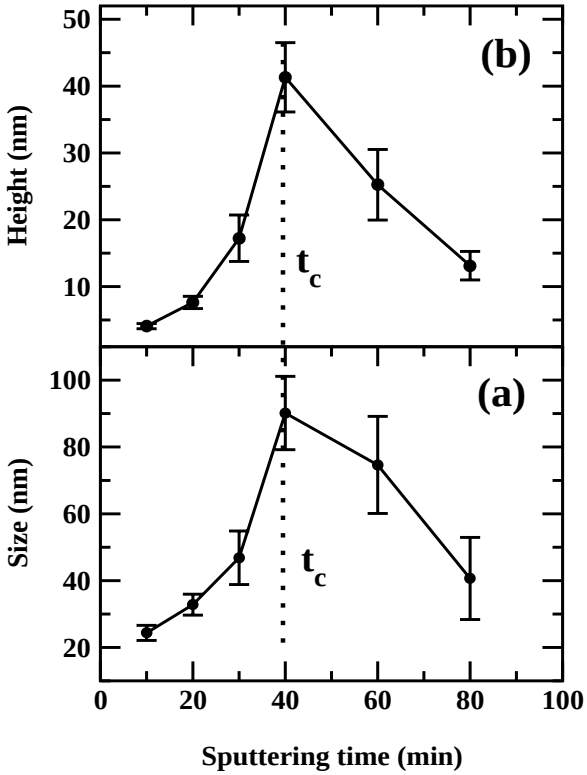

Figure 3. Mean size (a) and mean height (b) of the nanostructures formed after sputtering with 3 keV Ar^+ beam at various time intervals.

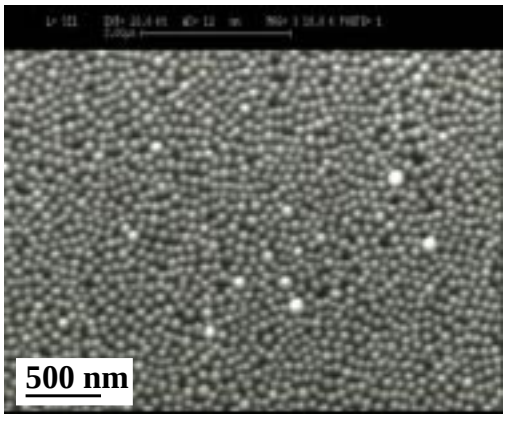

Figure 4. SEM image showing 3 μm × 3 μm pattern of self-assembled nano dots formed after sputtering with 3 keV Ar^+ beam for 40 min.

of agglomeration, the density of the dots decreases to 4 × 10^{10} cm^{-2} .

After 40 min. sputtering, SPM image displays an array of rectangular shaped cells as shown in Fig. 4. The spatial distribution of these dots appears very uniform with the rectangular dots arranged in rows. Figure 4 shows the SEM image taken on large area after 40 min sputtering where the ordering of the self assembled InP nano dots can be clearly seen. The process of ripening and agglomeration of dots continues causing further increase in the size and the height of the dots and a decrease in their density. Figs 2 and 3 show immense increase in the size and the height of the dots at this stage with their average size and height becoming 90 nm and 41 nm, respectively. Dot smaller than 40 nm or lower than 25 nm are not observed. The density of the dots is observed to be 6 × 10^9 cm^{-2}. Table 1 lists the density, mean size and mean height of the nano-structures at the various sputtering times:

During the coarsening, when the dots grow, the size (and height) distributions becomes broader (Fig. 2 (b),(c),(d)) and although the dots continue to exist, the local order in their pattern, which was present at 10 min, becomes weaker. Autocorrelation or Fast Fourier Transform approach can delineate the repeating patterns and gives signatures of surface ordering. The nano dot patterns obtained at 10 min display self-organization (Fig. 1(c)) with short range weak square order as revealed by 2-D auto-correlation pattern in Fig. 5(a). The local order, though still weak becomes better at 40 min. SPM image (Fig. 1(f)) exhibits a self assembly of rectangular celled arrays and the 2D auto-correlation pattern displays a short range weak square ordering in Fig. 5(b).

Interestingly, for sputtering durations higher than 40 min, a combination of inverse ripening and fragmentation

Table 1. Density, size and height distribution of nano-structures

Time (min)	Density (cm^{-2})	Size (nm)	Height(mn)
10	2 × 10^{11}	24 ± 4	4 ± 0.4
20	2 × 10^{11}	33 ± 5	8 ± 0.9
30	4 × 10^{10}	47 ± 16	17 ± 3
40	6 × 10^9	90 ± 26	41 ± 5
60	3 × 10^{10}	75 ± 37	25 ± 5
80	4 × 10^{10}	41 ± 14	13 ± 2

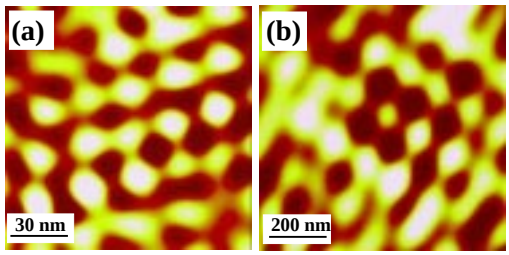

Figure 5. Auto-correlation pattern after (a) 10 min sputtering from 150 nm × 150 nm SPM image and (b) 40 min sputtering from 1000 nm × 1000 nm SPM image.

of nano dots is observed. Fig. 1(g). displays the fragmentation of several bigger dots into smaller dots after 60 min. sputtering. As a consequence, the density of dots increases to 3×10^{10} cm^{-2} and the size of the dots reduces. The dots have an average size of 75 nm compared to 90 nm seen after 40 min. of sputtering. The average height of the dots also reduces to 25 nm compared to 41 nm after 40 min. sputtering Fig. 3. Moreover, small dots of sizes 20 nm and height 5 nm are seen at this stage Fig. 2(e), which were not seen after 40 min. The decrease in height suggests that the inverse ripening may not just happen due to the fragmentation of dots, due to sputtering, into smaller sizes but some mass flow from larger to smaller dots may also be involved. Both size and the height distributions are very broad at this stage. Existence of some large 200 nm nano dots suggests that a few dots may also ripen at this stage. However, there numbers is very small and fragmentation and inverse ripening dominates the structure formation. SPM images show that the fragmentation and inverse ripening of nano dots continues after 80 min of sputtering also (Fig. 1(h)). This causes a further decrease in size and height of nano dots as well as an increase in their density to 5×10^{10} cm^{-2}. The average size and the height of the dots are 41 nm and 13 nm, respectively.

Figure 6 shows the rms roughness of the InP surfaces with nano-dots. During the early stages of sputtering process, the rms roughness increases from 0.5 nm for the virgin sample to 5.5 nm after sputtering for 40 min. However, for higher sputtering durations the roughness decreases to about 3.0 nm after 80 min. Thus, during the coarsening of nano dots from 10 to 40 min the surface roughens whereas when the fragmentation and inverse-coarsening of the nano-dots occurs, beyond 40 min, a slight smoothening in the surface is observed. The time (40 min or the fluence 24 $\times 10^{15}$ ions/cm^2) beyond which a slight decrease in rms surface roughness is observed is referred to here-after as critical time, t_c . Smoothening of surface beyond the critical time as discussed later is associated with the amorphization of the surface at this stage. At high ûuences, the density of electronic excitations increases and the covalent bonds

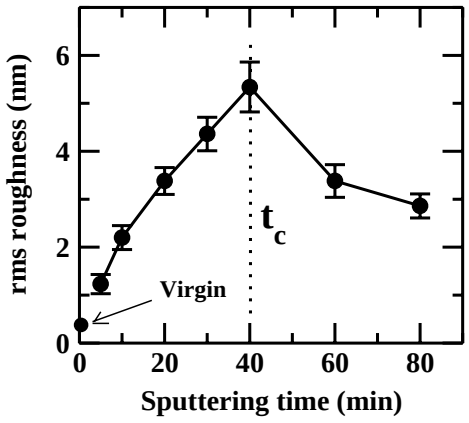

Figure 6. Variation of rms surface roughness and spatial wavelength are plotted as a function of sputtering time for irradiation with 3 keV Ar^+ beam.

in the lattice weaken or get broken causing the surface-amorphization. The amorphization can lead to relaxations[30,31] and smoothening of the surface via decreased strains[32]. Surface smoothening has been reported for MeV *Sb* ion implantation in *Si*[33] and InP[34] as well as for keV implantations of *P* and *As* in amorphous films[35].

For III-V semiconductors like InP and other zinc- blend structures, the ûrst order Raman spectrum consists of usually two Raman modes corresponding to the Longitudinal Optical (LO) and Transverse Optical (TO) phonons associated with the Brillouin zone center. The zone center phonons corresponding to TO and LO modes obey the following selection rules for zinc blend type crystals. For the scattering by (111) face, both LO and TO modes are allowed in Raman scattering. However, only TO mode is allowed for scattering by (110) face whereas only LO mode is allowed for (100) face. Both LO and TO modes being allowed for InP(111), we have been able to investigate the evolution of both these modes at various sputtering influences. Raman spectra from virgin (bulk) InP and nano patterned InP surfaces after Ar^+ ion sputtering are shown in Fig. 7. LO and Transverse Optical (TO) modes appearing at 351.5 cm^{-1} and 301.5 cm^{-1}, respectively, for the virgin sample, soften and shift towards lower wave-numbers appearing at 350.5 and 300.5 cmd1, respectively, for 5 min sputtering. The softening of the modes, suggests development of tensile stress after sputtering[32]. Due to the Frohlich interactions[36], LO is a more surface sensitive mode and thus its modfications may reflect the structural changes on the InP surface[37]. The LO mode shifts to 350.2, 350.3 and 349.2 cm^{-1} after 10, 20 and 30 min, respectively, with the largest shift being 2.3 cm^{-1} after 30 min. The surface, thus, is under tensile stress that increases with time up to 30 min. The assymmetricity seen in LO

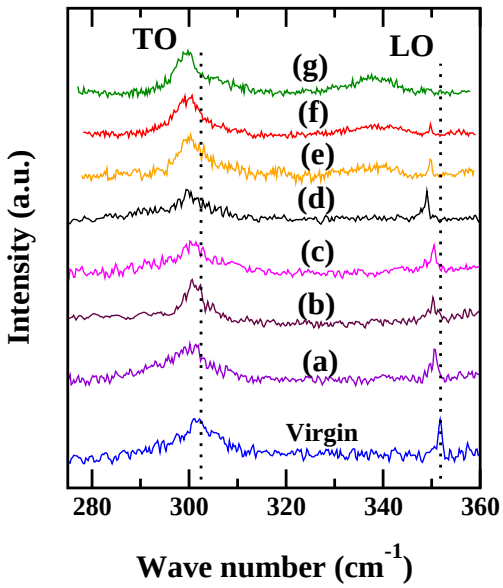

Figure 7. Raman Spectra of virgin InP and 3 keV sputtered InP surfaces after sputtering for (a) 5 min, (b) 10 min, (c) 20 min, (d) 30 min, (e) 40 min, (f) 60 min, and (g) 80 minutes.

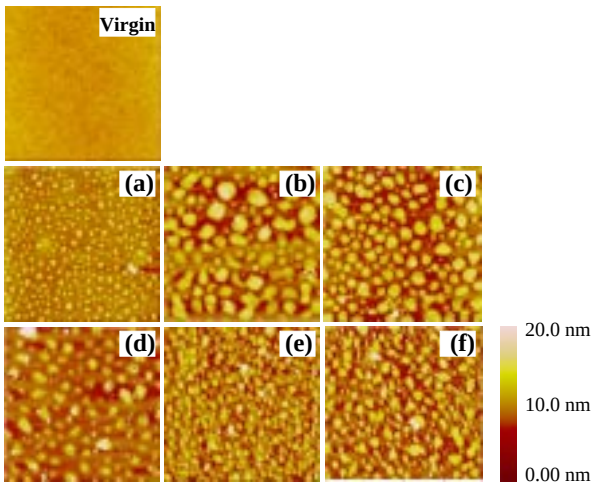

Figure 8. 10 × 10¼ m² SPM images of InP surfaces for the virgin sample as well as after implantation with 1.5 MeV *Sb* ions at a fluence of (a) 1×1011 ions/cm² , (b) 1×10¹² ions/cm², (c) 1 × 10¹³ ions/cm² , (d) 1 × 1014 ions/cm², (e) 5 × 10¹⁴ ions/cm² . and (f) 1 × 10¹⁵ ions/cm² enter.

modes can be attributed to the phonon confinement effects in nanodots[37]. At t_c, a reduction in shift to 1.8 cm^{-1} (LO feature at 349.7 cm^{-1}) suggests a slight relaxation in stress. A significant decrease in the LO intensity is also noticed at t_c. The reduced stress, lower LO intensity as well as the appearance of a broad feature at 340 cm^{-1} suggest the initiation of amorphization at the InP surface at this stage (fluence of 24 × 10^{15} ions/cm^2)[38]. With the surface beginning to amorphize at t_c, the surface becomes completely amorphous at 80 min where no LO feature but a stronger 40 cm^{-1} feature is present[38]. This surface-amorphization also leads to smoothening of the surface seen in Fig. 6.

3.2 Nano-Patterning by MeV Ion Irradiation

Figure 8 shows the 10×10 μm^2 2D SPM images from the InP surfaces. The image from a virgin (un-implanted) InP(111) sample is shown and it is observed that this surface is smooth. Other images of Fig. 8 show the evolution of the surface morphology on InP surfaces after 1.5 MeV *Sb* implantation at fluences ranging from 1×10^{11} ions/cm^2 to 1×10^{15} ions/cm^2. Comparison of the surface morphologies of InP surfaces of Fig. 8, after implantation, show the formation of nanoscale sized defects with varying size, height and density depending on the ûuence. Fig. 8(a) shows the InP surface after an *Sb* implantation with 1×10^{11} ions/cm^2. Several nano sized defects can be observed on the surface. The structures have developed due to the damage created at the surface. We have investigated the height and the size distributions of the nanoscale sized defects (seen in Fig. 8) on the InP surfaces after various *Sb* fluences. The size and the height distributions are shown in Figs. 9 and 10, respectively. After a fluence of 1×10^{11} ions/cm^2, most of the nanostructures have a diameter smaller than 450 nm and a height smaller than 10 nm. The density of the nanostructures

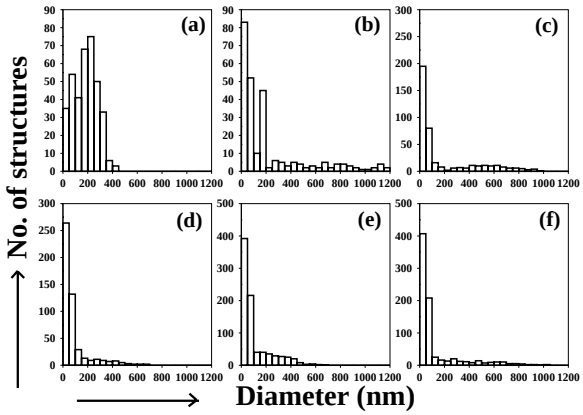

Figure 9. Size distributions of the surface structures after 1.5 MeV *Sb* implantation with fluences of (a) 1 × 10¹¹ ions/cm², (b) 1 × 10¹² ions/cm², (c) 1 × 10¹³ ions/cm², (d) 1 × 10¹⁴ ions/cm², (e) 5 × 10¹⁴ ions/cm², and (f) 1 × 10¹⁵ ions/cm²

has been calculated to be about 2.5×10^8 cm^{-2}.

Fig. 8(b) shows the InP surface image after an *Sb* ûuence of 1×10^{12} ions/cm^2 . We ob-serve that the nanostructures have become bigger in size. As seen in the size distribution of Fig. 9(b), some structures have diameter as large as 1200 nm. However, a large number of nanostructures have diameter smaller than 200 nm. Although some nanostructures are as high as 18 nm, most of the nanostructures are lower than 12 nm (Fig. 10(b)). Furthermore, a large number of nanostructure have a height lower than 4 nm. The density of the nanos-tructures is found to be similar to that observed at 1×10^{11} ions/cm^2. At 1×10^{13} ions/cm^2, in Fig. 8(c), we notice a slight increase in the density of nanostructures to 3.6×10^8 cm^{-2}. A few nanostructures have diameters as large as 950 nm. A large number of nanostructures, greater than at 1×10^{12} ions/cm^2, have diameters smaller than 200 nm (Fig. 9(c)). Although some are 20 nm high, a large number have a height lower than 12 nm (Fig. 10(c)). Again,

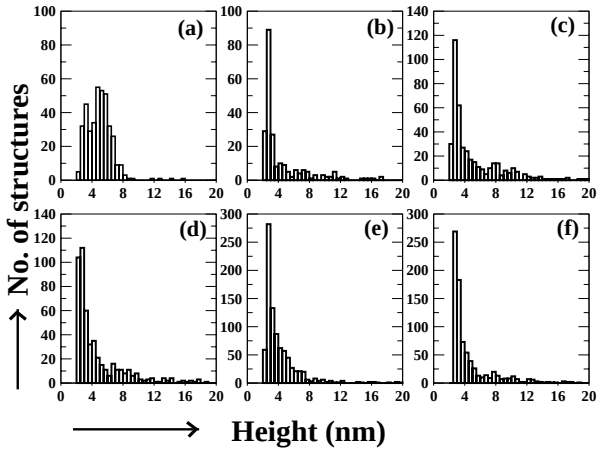

Figure 10. Height distributions of the surface structures after 1.5 MeV *Sb* implantation with fluences of (a) 1 × 10¹¹ ions/cm², (b) 1 × 10¹² ions/cm², (c) 1 × 10¹³ ions/cm², (d) 1 × 10¹⁴ ions/cm², (e) 5 × 10¹⁴ ions/cm² and (f) 1 × 10¹⁵ ions/cm².

a large number of nanostructures have a height lower than 4 nm. The increase in density at this stage can also be noticed by a changed (y) scale for both the distributions. Fig. 8(d) shows the image acquired after the ûuence of 1×10^{14} ions/cm^2. The density of the nanos-tructures is about 5.0×10^{8} cm^{-2} . The size and the height distribution is very similar to that observed at 1×10^{13} ions/cm^2 . However, the diameter of the largest nanostructures observed is smaller (700 nm) and the number of small (diameter less than 100 nm) nanostructures has increased (Fig. 9(d)). Also, larger number have a height lower than 4nm (Fig. 10(d)).

After a fluence of 5×10^{14} ions/cm^2 , a drastic increase in density of the nanostructures is observed in Fig. 8(e). We also observe a larger number of nanostructure with small size. The density of nanostructures at this stage is about 8.0×10^{8} cm^{-2} . Although the size distribution is similar to that observed at 1×10^{14} ions/cm^2 , the re are many more nano-structures with small 0-100 nm diameter (Fig. 9(e)). Similarly the nanostructures having height smaller than 4 nm has increased (Fig. 10(e)). The SPM image after a fluence of 1×10^{15} ions/cm^2 is shown in Fig. 8(f). The density of the nanostructures, 8.0×10^{8} cm^{-2}, as well as the size and the height distributions are very similar to those observed after 5×10^{14} ions/cm^2. However, some structures of large 1000 nm diameter (Fig. 9(f)) are also seen. Similar size and height distributions were also observed for 5×10^{15} ions/cm^2. Here we notice that for all fluences,the defect density is far lower than the ion beam ûuence. Possible reasons for this will be discussed below.

Figure 11 shows the high resolution 1×1 μm^2 , 0.5×0.5 μm^2 and 0.2×0.2 μm^2 images of the InP(111) surfaces after the ûuence of 1×10^{13} ions/cm^2 and 5×10^{14} ions/cm^2 . The figures show that the InP(111) surfaces are very diûerent, at each scale, for these two fluences. Some SPM-sections with images are shown in Fig. 12 to display some characteristic features of the distribution of the defects on InP surfaces. Fig. 12(a) shows a 1.0×1.0μm^2 SPM image of InP surface

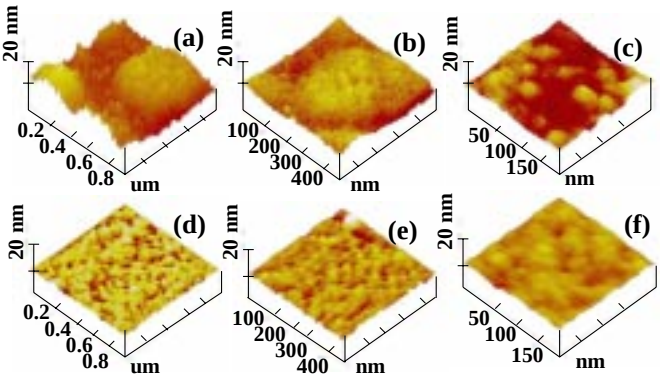

Figure 11. InP surface SPM images (a) 1 × 1 μm², (b) 0.5 × 0.5 μm² and (c) 0.2 × 0.2 μm² after implantation at fluence of 1 × 10¹³ ions/cm². Images (d) 1 × 1 μm², (e) 0.5 × 0.5 μm² and (f) 0.2 × 0.2 μm² are after implantation at fluence of 5 × 10¹⁴ ions/cm². For all images implantation was performed with 1.5 MeV *Sb* beam.

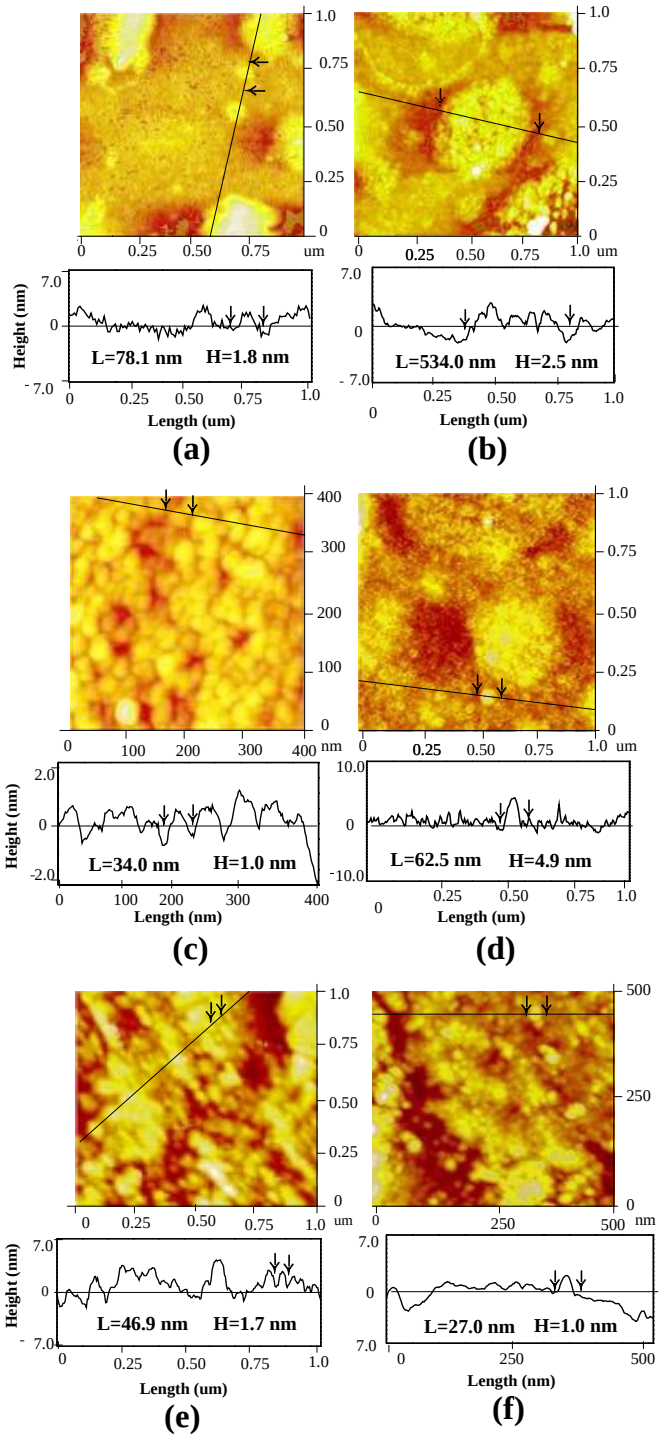

Figure 12. InP surface SPM images and SPM-section analysis of (a) 1 × 1 μm² image for 1 × 10¹¹ ions/cm² (b) 1.0 × 1.0 μm² image for 1 × 10¹² ions/cm² (c) 0.4 × 0.4 μm² image for 1 × 10¹² ions/cm² (d) 1 × 1 μm² image for 1 × 10¹³ ions/cm² (e) 1 × 1 μm² image for 5 × 10¹⁴ ions/cm² (f) 0.5 × 0.5 μm² image for 1 × 10¹⁵ ions/cm² (L is the lateral dimension and H is the height of the nanostructure labelled with arrows)

after an ion fluence of 1×10^{11} ions/cm^2 along with the section analysis demonstrating a defect of 78.1 nm lateral and 1.8 nm vertical dimensions. Some defects of smaller size and height are also visible. Fig. 12(b) shows 1.0×1.0 μm^2

SPM image of InP surface after an ion ûuence of 1×10^{12} ions/cm^2. Some small and big sized defects are visible. Section analysis of a defect with dimensions 534 nm in lateral and 2.5 nm in vertical direction is also shown. We interestingly notice that this defect is actually composed of several smaller defects. These features can be clearly seen in Fig. 12(c) where a high resolution 0.4×0.4 μm^2 SPM image of this defect (from Fig.12(b)) is shown. To emphasize, image in Fig. 12(c) shows the internal structure of the big defect analyzed in Fig. 12(b). As seen in Fig. 12(c), the smaller defects embedded in the big defect are of several sizes and heights. Section-analysis of a typical small defect is shown in Fig.12(c) with dimensions of 34.0 nm in lateral and 1.0 nm in the vertical direction. The image also shows that several defects are overlapping other defects. Fig. 12(d) shows a 1.0×1.0 μm^2 SPM image for a ûuence of 1×10^{13} ions/cm^2 . The section analysis shows a defect of 62.5 nm lateral and 4.9 nm vertical dimensions. Again, the big defects clearly appear to be composed of several smaller defects. Several small and lower defects can also be seen spread over the surface. Similar behaviour is also noticed in Fig. 12(e) where a 1.0×1.0 μm^2 SPM image is shown for a fluence of 5×10^{14} ions/cm^2. The bigger defects are fully embedded with several smaller defects of various heights. The section analysis shows a defect with 46.9 nm lateral and 1.7 nm vertical dimensions. A big defect is shown in a 0.5×0.5 μm^2 image of Fig.12(f) for a fluence of 1×10^{15} ions/cm^2. Here also the big defect is embedded with several smaller defects. The section analysis shows a defect with 27.0 nm lateral and 1.0 nm vertical dimensions. Several smaller defects can also be seen around the big defect. These images show that the bigger defects at all fluences are embedded with several of nanosized defects. During the investigation of 10×10 μm^2 images of Fig.8, we had noticed that the density of defects for all fluences varies between $2.5\text{-}8.0\times10^8$ cm^{-2} which is much lower compared to the ion ûuences. From Fig. 12, we notice that the bigger defect structures are composed of smaller nanosized-defects of sizes ~ 30 nm. Taking this fact into account we have recalculated the density of defects and find it to be 5.0×10^{10} cm^{-2} at 1×10^{11} ions/cm^2 and 1 - 1.5×10^{11} cm^{-2} for higher fluences. We further notice, in Figs. 10 and 12, that the height of defects also vary as a function of fluence. Although, most of the defects are about 4 nm high, higher defects are also increasingly seen at larger fluences Fig. 10. In the framework of model introduced by Gibbons[39], the amorphous material is produced either directly by a single incoming ion or by multiple overlaps. According to this model, the ratio between the total surface area A_A covered by damages and the total area A_0 being implanted is given by

$$\frac{A_A}{A_0} = 1 - e^{-A_1\phi} \sum_{k=0}^{m} \frac{A_1\phi^k}{k!}$$

where $A_1 = \pi r_m^2$ is the surface area damaged by a single ion impact, ϕ is the fluence and m is the overlap number. For 1×10^{11} ions/cm^2 with r_m of 30 nm we found that m is 2, i.e. about two ions must impinge on the same area to produce the defect. For 250 MeV Xe irradiation of InP, Herre et al. find that the values of m is between 2 and 3[40]. Higher heights of defects for larger fluences, as observed in Fig. 10, may denote larger m. In addition, more than one defect may be getting formed at one place. Overlapping defects as well as defects smaller than 30 nm have also been seen in Fig. 12. All these factors together can be responsible for the observation of the lower defect density than the ion fluences.

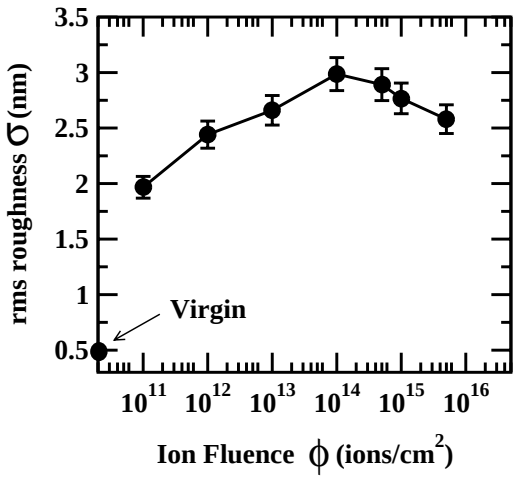

Figure 13. The rms surface roughness (σ) of the *Sb* implanted InP(111) surfaces, measured using SPM, is plotted as a function of *Sb* ion fluence. Data for the virgin sample is also shown.

We have also studied the rms surface roughness of the InP surfaces after MeV ion implantation. In Fig. 13 we have plotted the rms surface roughness (σ) of the InP surfaces as a function of ion fluence. For a virgin InP(111) surface, σ was measured to be 0.47 nm and is also marked in Fig. 13. We observe that the rms surface roughness exhibits two distinct behaviors as a function of fluence. Initially up to 1×10^{14} ions/cm^2 , σ increases with the increasing fluence. However for higher fluences σ decreases for increasing fluences. Our results show that there is a critical fluence of 1×10^{14} ions/cm^2 , below which the rms roughness of the InP surfaces increases with ion fluence whereas for higher fluences the surface roughness decreases with increasing fluences. This behaviour is similar to that observed for 3 keV irradiation of InP discussed, in Fig. 6, where also an initial increase in surface roughness upto a critical time and then a decrease in roughness for higher durations was observed. The critical fluence, 24×10^{15} ions/cm^2 (critical time=40 min) is, however larger for keV irradiation. A decrease in surface roughness with increasing fluence, beyond a critical fluence, has also been observed for MeV *Sb* implantation in *Si* (100)[33] and for keV implantations of P and As in amorphous films[35].

Figure 14 shows the as-implanted Raman spectra from the InP samples implanted with various *Sb* doses. All these

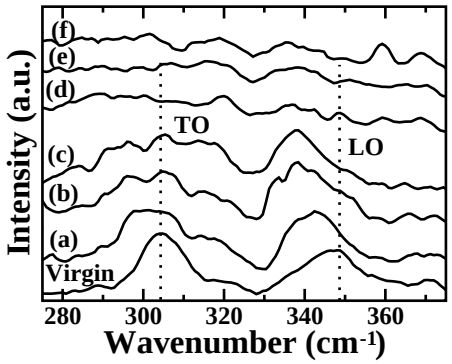

Figure 14. Raman spectra are shown for virgin InP(111) as well as after 1.5 MeV *Sb* implantation of InP with various fluences of (a) 1 × 10^{11}, (b) 1 × 10^{12}, (c) 1 × 10^{13} (d) 1 × 10^{14}, (e) 5 × 10^{14} and (f) 1 × 10^{15} ions/cm^2. The curves are vertically displaced for clarity.

spectra were acquired in the backscattering geometry. As the penetration depth of the light is much smaller than the projected range of the implanted *Sb* ions, Raman scattering results are primarily from the surface region. The spectrum from a virgin (un- implanted) InP is also shown for comparison. The spectra have been shifted vertically for clarity, but the intensity scale is the same for all the spectra. The spectrum of the virgin InP (Fig.14) shows the characteristic longitudinal optical (LO) and transverse optical (TO) Raman peaks of crystalline InP(111)[41]. The features at 305 cm^{-1} and at 347 cm^{-1} are assigned to the TO and the LO phonon modes, respectively. The sequence of spectra gradually evolve, with increasing fluence, from the characteristic crystalline InP(111) spectrum to the amorphous like spectrum of Fig. 14(f). The spectrum for the 1×10^{11} ions/cm^2 sample (Fig. 14(a)) exhibits some changes when compared to virgin InP. We observe that in addition to the shifts of both LO and TO features towards the lower wave numbers, TO feature also exhibits an asymmetric broadening towards the lower wave numbers. All these changes reflect the modifications in the InP due to the defects created during implantations. After a fluence 1×10^{12} ions/cm^2 (Fig. 14(b)) we observe a decrease in the intensity of the TO mode. In addition, broadening as well as the shifts towards lower wave numbers are observed, for both LO and TO modes. Spatial Correlation model related to q-vector relaxation induced damage shows[42] that when disorder is introduced into the crystal lattice by implantation, the correlation function of the phonon-vibrational modes becomes finite due to the induced defects. Consequently the momentum q=0 selection rule is relaxed. Consequently, the phonon modes shift qualitatively to lower frequencies and broaden asymmetrically as the ion fluence is increased[43]. Thus the shifts to lower frequencies as well as the asymmetrical broadening of the features, observed in Fig. 14, are due to the residual defects created due to S_n during ion implantation. Accordingly, these two features are also referred to as DALO and DATO respectively for disorder activated (LO) and (TO) modes. The shifts, of the LO and TO modes, towards the lower wave numbers also indicate the development of the tensile strain in the lattice. Our results are in contrast to the studies of Si^+ implantation in InP at 150 keV[44] where no noticeable changes compared to the virgin InP were seen up to the fluence of 1×10^{12} ions/cm^2 and the first signatures of disorder were observed after the fluence of 5×10^{12} ions/cm^2. For 2 MeV *Se* implantation in InP, however, some damage after 1×10^{12} ions/cm^2 has been reported using channeling experiments[45].

In Fig.14(c) after a fluence of 1×10^{13} ions/cm^2 , a further decrease in the TO mode intensity as well as increased broadening and shifts of LO, TO modes towards smaller wave numbers are observed. After a fluence of 1×10^{14} ions/cm^2, the Raman spectrum (Fig. 14(d)) exhibits no distinct features corresponding to LO or the TO modes indicating that at this stage the lattice has been amorphised. The DATO and DALO structures have become completely merged into a broad band containing the whole density of states of the optical modes. This spectrum resembles that of amorphous InP[46]. Hence, we notice that InP has become amorphised at 1×10^{14} ions/cm^2 and further increase of ûuences does not produce changes in the LO or TO modes (Fig. 14(e), 14(f)). Since the penetration depth of Ar^+ laser is 100 nm in InP (range of *Sb* ions being 400 nm), the Raman results here are primarily from surface region. The decrease in rms surface roughness, σ, (Fig. 13) can thus be related to the amorphization of the InP at this fluence. The amorphization can lead to relaxations[30,31] and smoothening of the surface via decreased strains[32]. The ion bombardment produces the erosion at the surfaces and also leads to the formation of surface structures. For low energy, keV sputterings, this is primarily controlled by the Nuclear energy loss (S_n) due to the elastic collision of the ions with the atoms in the solid. The arrival of the ions on the surface is a stochastic process. Moreover, with the sputtering events being of varying magnitudes and being spatially distributed, the surfaces sometimes display surface structures during ion bombardment. At MeV scales, the eflect of S_n is very small and electronic energy loss (S_e) due to the inelastic collisions of ions with electrons of the solids are appreciable. The Swift Heavy ion (SHI) studies on semiconductor materials have, however, shown that S_e is insensitive in creating defects the bulk lattice. Some studies have further shown that S_e can sometimes lead to the annealing of defects produced via the Sn process. The ion bombardment of the semiconductor surface, in addition to forming surface structures can also roughen and amorphize it depending on the target, ion and its energy. The mechanism and the evolution of the roughening of a crystalline surface depend on several competing factors controlled by the ion energy and the target characteristics. Irradiation induced mass-ûow, dangling bond induced flow, S_n induced sputtering, radiation enhanced diflusion, surface diflusion and stoichiometric modifications due to preferential sputtering in compound semiconductors are some of the factors influencing the surface morphology and its roughening behaviour[47].

Comparing the 1.5 MeV irradiation results with the keV irradiation results shown in Fig. 6, we observe that

upto the fluence of 5×10^{15} ions/cm^2 (maximum fluence studied for MeV irradiation) the rms surface roughness is smaller for keV irradiation of InP surfaces. Since the surface roughness is expected to be primarily controlled by the S_n, higher rms roughness for MeV irradiated (S_n = 2 keV/nm, S_e = 1 keV/nm) surfaces compared to keV sputtered S_n = 0.34 keV/nm, S_e = 0.05 keV/nm) surfaces is expected. Moreover, when comparing with the study of 100 MeV Au SHI irradiation[48] on InP (S_n = 378 eV/nm, S_e = 15 keV/nm), we expect a higher surface rms roughness at all fluences for the 1.5 MeV irradiated samples, studied here, as the S_n is higher[27]. Although for fluences upto 1×10^{13} ions/cm^2 this is seen, for 1×10^{14} ions/cm^2 we observe a lower roughness in our case. This is an unexpected result and suggests that at higher fluences factors other than Sn are also playing role. At high fluences, density of electronic excitations increase, covalent bonds in the lattice weaken or get broken. As a result the lattice softens. This softening of the bonds and amorphization of the InP lattice occurs at the critical fluence as shown by the Raman scattering results. The SHI studies[48] did not investigate the fluences higher than 1×10^{14} ions/cm^2 and also did not observe any decrease in the roughness. The critical fluence (24×10^{15} ions/cm^2)seen after 3 keV irradiation, in the present study, is at a higher fluence than that seen here after 1.5 MeV irradiation (1×10^{14} ions/cm^2). Small contribution of S_n, at 3 keV compared to that at 1.5 MeV, requires a higher fluence for the surface amorphization. The surfaces undergo the amorphization at the critical fluence and displays smoothening at higher fluences. Thus, S_n related processes, differential sputtering of a component, and the presence of tensile stress as observed in Raman spectra by softening of LO, TO modes, may be all together responsible for creating the nano-sized structures observed here. Furthermore, the theoretical model show that the surface roughness, created via nano-patterning, should saturate at long time scales. However, patterning of InP surfaces, both at keV and MeV energies, as studied here show that the surface roughness decreases, instead of saturating at long time durations. This demonstrates the need for including higher order non-linear terms in the theoretical models.

4. SUMMARY AND CONCLUSIONS

In conclusion, ion irradiation is a powerful technique to modify the surfaces. The self assembled growth that takes place on the ion irradiated surface strongly depends on the energy of the irradiation. After low (3 keV) energy irradiations, InP surfaces display nano dots on the surface. These self assembled structures are a result of competition between the curvature dependent erosion and diffusion mediated smoothening phenomenon undergoing on the surface during irradiation. Surface behavior thus becomes complex with surface roughness and surface stress varying with fluence, erosion and diflusion of atoms. The MeV implantation also leads to formation of nanostructures on the surface. These structures are, however, defect zones created by high energy irradiation. Although the self assembled structures and their distributions vary with energy, as has been observed in the present study, some salient features are common. For both the low energy (keV) and the (MeV) irradiations the surface initially roughens but then smoothens beyond a critical fluence. At the critical fluence the surface undergoes a/c transitions and smoothens the surface for higher fluences. The surface amorphization also causes relaxation of the stress on the surface.

5. ACKNOWLEDGEMENTS

Authors would like to acknowledge the help of Mr Santosh Choudhury in sputtering experiments and Mr Vanaraj Solanki for write up.

REFERENCES

1. Streit, D. Indium phosphide ICs in strong demand for 40 Gbit/s networks. *Compound Semiconductors,* May 2002.
2. Humphreys, B. & O'Donell, A. A building block approach to manufacturing monolithic photonic integrated circuits. *Compound Semiconductors*, August 2003.
3. Lammers, D. Cygnal: Proof it can be done. *Electronic Engineering Times*, 12 September 2002.
4. Andrew, N.; Shipway, Eugenii Katz. & Itamar, Willner Nanoparticle Arrays on Surfaces for Electronic, Optical, and Sensor Applications. *Chem Phys Chem*, 2000, **1**(1) 18-52.
5. Sigmund, Peter. Theory of Sputtering. I. Sputtering Yield of Amorphous and Polycrystalline Targets. *Phys. Rev.* 1969, **184** (2), 383-416.
6. Mark Bradley, R. & James, M. & Harper, E. Theory of ripple topography induced by ion bombardment. *J. Vac. Sci. Technol. A,* 1988, **6** (4) 2390-395.
7. Demanet C. M. *et al*., Atomic force microscopy investigation of argon-bombarded InP: Effect of ion dose density. *Surf. Interface Anal.* 1995, **23**(7-8), 433-39; 1996 **24**(8), 497-502; 1996, **24**(8), 503-10.
8. Facsko, S.; Dekorsy, T.; Koerdt, C.; Trappe, C.; Kurz, H.; Vogt, A.& Hartnagel, H. L. Formation of Ordered Nanoscale Semiconductor Dots by Ion Sputtering, Science, 1999, **285**(5433), 1551-553.
9. Kahng, B.; Jeong H. & Barabasi, A.-L. Quantum dot and hole formation in sputter erosion. *Appl. Phys. Lett.* 2001, **78**(8), 805-07.
10. Tan, S.K. & Wee, A.T.S. Self-organized nanodot formation on InP(100) by argon ion sputtering at normal incidence. *J. Vac. Sci. Technol. B*, 2006, **24**(3), 1444-448.
11. Frost, F.; Schindler, A. & Bigl, F. Roughness Evolution of Ion Sputtered Rotating InP Surfaces: Pattern Formation and Scaling Laws. *Phys. Rev. Lett.*, 2000, **85**(19), 4116-119.
12. Ziberi, B.; Frost, F. & Rauschenbach, B. Pattern transitions on Ge surfaces during low-energy ion beam erosion. *Appl. Phys. Lett.*, 2006, **88**(17), 173115-73118.
13. Maclaren, S.W.; Baker, J.E.; Finnegan, N.L. & Loxton, C.M. Surface roughness development during sputtering of GaAs and InP: Evidence for the role of surface

diffusion in ripple formation and sputter cone development. *J. Vac. Sci. Technol. A*, 1992, **10**(3), 468-76.

14. Frost, F.; Ziberi, B.; Hoche, T. & Rauschenbach, B. The shape and ordering of self-organized nanostructures by ion sputtering. Proceedings of the E-MRS 2003 Symposium E on Ion Beams for Nanoscale Surface Modifications. *Nucl. Instr. and Meth. B,* 2004, **216**, 9-19.
15. Cuerno, R. & Barabasi, A. L. Dynamic Scaling of Ion-Sputtered Surfaces. *Phys. Rev. Lett.*, 1995, **74**(23), 4746-749.
16. Makeev, M. A. & Barabasi, A. L. Ion-induced effective surface diffusion in ion sputtering. *Appl. Phys. Lett.*, 1997, **71**(19), 2800-03; M. A. Makeev, R. Cuerno, and A. L. Barabasi,Morphology of ion-sputtered surfaces. *Nucl. Instrum. Methods Phys. Res. B*,2002, **197**(3-4), 185-227.
17. Kuramoto, Y. & Tsuzuki, T. Persistent Propagation of Concentration Waves in Dissipative Media Far from Thermal Equilibrium. *Prog. of Theo. Phys.* 1976, 55(2), 356-369 Sivashinsky, G. I. On self-turbulization of a laminar flame. *Acta Astronaut.*, 1979, **6**(5-6), 569-91.
18. Park, S.; Kahng, B.; Jeong, H. & Barabasi, A.L. Dynamics of Ripple Formation in Sputter Erosion: Nonlinear Phenomena. *Phys. Rev. Lett.*, 1999, bf **83**(17), 3486-489.
19. Rost, M. & Krug, J. Anisotropic Kuramoto-Sivashinsky Equation for Surface Growth and Erosion. *Phys. Rev. Lett.*, 1995, 7**5**(21), 3894-3497.
20. Kardar, M.; Parisi, G. & Zhang, Y.-C. Dynamic Scaling of Growing Interfaces. *Phys. Rev. Lett.*, 1986, **56**(9), 889-92.
21. Tempel, G.; Schwarz, N.; Muller, F.; Koch, F.; Zeindl, H.P. & Eisele, I. Infrared resonance excitation of ?-layers-a silicon-based infrared quantum-well detector. *Thin Solid Films,* 1990, **184**(1-2), 171-76.
22. Bishop, S.G.; Shanabrook, B.V.; Klein, P.B. & Henry, R.L. New isoelectronic trap: Antimony in indium phosphide. *Phys. Rev. B.*, 1988, **38**(12), 8469- 472.
23. Tamura, M. & Suzuki, T. Damage formation and annealing of high energy ion implantation in Si. *Nucl. Instr. and Meth. B,* 1989, **39**(1-4),318-29.
24. Carter, G.; Nobes, M.J.; Katardjiev I.V. & Whitton, J.L. Defect and Diffusion Forum, Ion Implantation 1988, ed. F.H. Wohlbier (Trans. Techn. Publ. Ltd), 1988, vol.**57/58**, 97-126.
25. DiMaria D.J. & Kerr, D.R. Interface effects and high conductivity in oxides grown from polycrystalline silicon. *Appl. Phys. Lett.*, 1975, 27(9), 505.
26. Chu, W. K.; Mayer J. W. & Nicolet, M. A. Backscattering Spectrometry (Academic Press, New York, 1978).
27. Mehta, G.K. Swift heavy ions in materials science - emerging possibilities. *Vacuum,* 1997, **48**(12), 957-959.
28. Dey, S.; Kuri, G.; Rout B. & Varma, S. Range profiles and lattice location of MeV implant of Sb in Si (1 0 0). *Nucl. Instr. Meth. B,* 1998, **142**(1-2), 35-42.
29. Biersack J. P. & Haggmark, L. G. A Monte Carlo computer program for the transport of energetic ions in amorphous targets. *Nucl. Instr. and Meth. B,* 1980, **174**(1-2), 257- 69. We have used the version SRIM'03
30. Volkert, C.A. Stress and plastic flow in silicon during amorphization by ion bombardment. *J. Appl. Phys.*, 1991, **70**(7), 3521-3527 and reference therein.
31. Srivastava, P.C.; Ganesan, V. & Sinha, O.P. Evidence of plastic flow and recrystallization phenomena in swift (not, vert, similar100 MeV) Si7+ ion irradiated silicon. *Nucl. Instru. Methods, Phys. Res. B*, 2004, **222**(3-4), 491-96.
32. Dey, S.; Roy, C.; Pradhan, A. & Varma, S. Raman scattering characterization of Si(100) implanted with mega-electron-volt Sb. *J. Appl. Phys.* 2000, **87**(3), 1110-117.
33. Dey, S.: Paramanik, D.; Ganeshan, V. & Varma, S. Formation and Shape Transition of Nanostructures on Si(100) surfaces after MeV Sb Implantation. *Appl. Surf. Sci,* 2006, **253**(3), 1116-121.
34. Paramanik, D.; Pradhan A. & Varma, S. Nanoscale defect formation on InP (111) surfaces after MeV Sb implantation. *J. Appl. Phys.*, 2006, **99**(1), 014304-014311.
35. Edrei, R.; Shauly, E. N. & Hoffman, A. Influence of implantation and annealing on the surface topography of amorphous and polysilicon thin films . *J. Vac. Sci. Technol. A.*, 2002, **20**(2), 344-49.
36. Nash K.J. & Skolnick, M.S. Picosecond Raman studies of the Frhlich interaction in semiconductor alloys. *Phys. Rev. Lett.*, 1988, **60**(9), 863-63.
37. Paramanik D. & Varma, S. Raman scattering characterization and electron phonon coupling strength for MeV implanted InP(111). *J. Appl. Phy.*, 2007, **101**(2), 023528- 023535.
38. Cusco, R.; Talamas, G.; Artus, L.; Martin J.M. & Gonzalez-Diaz, G. Raman-scattering assessment of Si+-implantation damage in InP. *J. Appl. Phys.*, 1996, **79**(8), 3927-930.
39. Gibbons, J.F. Ion implantation in semiconductors Part II: Damage production and annealing. *Proc. IEEE*, 1972, **60**(9),1062- 096.
40. Herre, O.; Wesch, W.; Wendler, E.; Gaiduk. P.I.; Komarov, F.F.; Klaumunzer, S. & Meier, P. Formation of discontinuous tracks in single-crystalline InP by 250-MeV Xe-ion irradiation. *Phy. Rev. B.*, 1998, **58**(8),4832-837.
41. Pinczuk, A.; Ballman, A.A.; Nahory, R.E.; Pollack, M.A. & Worlock, J.M. Raman scattering studies of surface space charge layers and Schottky barrier formation in InP. *J. Vac. Sci. Technol.*, 1979, **16**(5), 1168-170.
42. Tiong, K.K.; Amritharaj, P.M.; Pollak F.H. & Aspens, D.E. Effects of As+ ion implantation on the Raman spectra of GaAs: Spatial correlation interpretation.

Appl.Phys. Lett., 1984, **44**(1), 122-125.

43. Richter, H.; Wang, Z.P. & Ley, L. The one phonon Raman spectrum in microcrystalline silicon. *Solid State Commun.*, 1981, **39**(5),625-29.
44. Cusco, R.; Talamas, G.; Artus, L.; Martin J.M. & Gonzalez-Diaz, G. Raman scattering assessment of Si+implantation damage in InP. *J. Appl. Phys*, 1996, **79**(8), 3927-3930.
45. Wesch, W.; Wendler, E.; Bachmann, T. & Herre, O. A comparative study of MeV and medium-energy ion implantation into IIIV compounds. *Nucl. Instru. Meth. Res. B.* 1995, **96**(1-2), 290-93.
46. Wihl, M.; Cardona M. & Tauc, J. Raman scattering in amorphous Ge and IIIV compounds. *J. Non-Cryst. Solids* **8-10**(Amorphous and Liquid Semiconductors), 1972, 172-78.
47. Eklund, E.A.; Snyder, E.J. & Williams, R.S. Correlation from randomness: quantitative analysis of ion-etched graphite surfaces using the scanning tunneling microscope. *Surf. Sci.*, 1993, **285**(3),157-80.
48. Singh, J.P.; Singh, R.; Mishra, N.C.; Kanjilal, D. & Ganeshan, V. Temperature dependent roughness of electronically excited InP surfaces. *J. Appl. Phys.*, 2001, **90**(12), 5968-973.

Contributors

Dr Dipak Paramanik is presently a postdoctoral researcher in Quantum Beam Center at National Institute for Material Science, Tsukuba, Japan. He did his MSc from Burdwan University, West Bengal, India, and PhD from Institute of Physics, Bhuaneswar, India. His PhD thesis was on Nano-structures formation on InP(111) semiconductor surfaces by ion beam irradiation. He was one of the Graduate Student awardees of the Material Research Society, USA in 2007. His research interests have been primarily in investigating surface modification and pattern formation on single crystal semiconductor surfaces using ion beam techniques, Scanning Probe Microscopy, Raman scattering, and X-ray photoelectron spectroscopy. He has published over 24 articles.

Mr Subrata Majumder is presently a Doctoral Research Scholar, working with Prof Shikha Varma, in the Experimental Condensed Matter Group at Institute of Physics, Bhubaneswar, India. He did his MSc in Physics from Visva Bharati University, India in 2005 and then joined the Doctoral program at Institute of Physics in 2006. His primary interests are in surface science, biological physics and dilute magnetic semiconductors. He has 5 publications.

Mr S.R. Sahoo is presently doing his PhD at Institute of Physics, Bhubaneswar under the supervision of Prof Shikha Varma. He passed his Masters Degree in Physics from Utkal University, Bhubaneswar, with specialization in Solid State Physics. His field of research is: Patterning of Semiconductor Surfaces using Ion beam Irradiation techniques. He joined the Ph. D program in 2006. He has 3 publications.

Dr Shikha Varma is presently an Associate Professor, in Condensed Matter Experimental Group at Institute of Physics, Bhubaneswar, India. She did her MSc from IIT Kanpur, India, and PhD from Syracuse University ,NY,USA. Her PhD thesis was on Interband Transitions in Thin overlayers of *Hg* on *Ag*(100): Angle Resolved UPS studies using ALLADIN and TANTALUS Synchrotron Sources. She was Postdoctoral fellow at Physics department Case Western University, Cleveland, USA and University of Wisconsin,Milwaukee, USA. She was also visiting Scientist at University of California, SantaBarbara, USA. She joined Institute of Physics, Bhubaneswar, as faculty in 1994. Her interests have been primarily in investigating electronic structure, topography and structural modifications of the single crystals, thin films, MBE-MOCVD grown structures and ion beam modified surfaces. She has published over 70 artcles.